Solution of the inverse scattering problem at fixed energy with non-physical S matrix elements

M. Eberspächer[1], K. Amos[1], and B. Apagyi[2]

[1] *School of Physics, The University of Melbourne, Parkville, Australia*

[2] *Institute of Physics, Technical University, Budapest, Hungary*

(December 13, 1999)

Abstract

The quantum mechanical inverse elastic scattering problem is solved with the modified Newton-Sabatier method. A set of S matrix elements calculated from a realistic analytic optical model potential serves as input data. It is demonstrated that the quality of the inversion potential can be improved by including non-physical S matrix elements to half, quarter and eighth valued partial waves if the original set does not contain enough information to determine the interaction potential. We demonstrate that results can be very sensitive to the choice of those non-physical S matrix values both with the analytic potential model and in a real application in which the experimental cross section for the symmetrical scattering system of $^{12}C+^{12}C$ at $E = 7.998$ MeV is analyzed.

03.65.N, 24.10.E, 24.10.H, 25.70.

I. INTRODUCTION

Solutions of quantum inverse scattering problems (ISP's) involve two step processes. In the first step, a set of S matrix elements, scattering phase shifts, and/or deflection functions are calculated from a given set of data, such as a differential cross section [1]. This process involves uncertainties as the measured data usually is incomplete [2,3] and, in any event, there exist natural ambiguities with any (even complete) fixed energy data [4]. We are not concerned with these matters in this paper and suppose that a *physical* S matrix can be defined. The adjective *physical* designates that the angular momentum quantum numbers identifying each and every number of the set are observable and/or contributing elements in summations leading to observables. The second step in solution of ISP's is the actual inversion process with which the underlying interaction is calculated from those S matrix elements. The result usually takes the form of a local potential matrix [5,6] which depends on the angular momentum or on the scattering energy according as one is solving the ISP at fixed angular momentum or at fixed energy. In the first case one needs as input data, the S matrix as a continuous function of energy at a fixed angular momentum and the energy values of any bound states. In the fixed energy ISP case the S matrix as a discrete function of the angular momentum variable is required.

Our interest is with the fixed energy ISP for which there are many quantal methods of solution; some of which are the Lipperheide and Fiedeldey (LF) methods [7], the finite difference method of Hooshyar and Razavy [8], and the generalized Darboux transformations of Schnizer and Leeb [9]. More recently, methods have been developed to incorporate the spin-orbit field cases, and examples are those of Huber and Leeb [10] who deal also with the Dirac equation as the equation of motion, and of Lun *et al.* [11] who found a linearization scheme. In this case, two sets of phase shifts or S matrices must be specified and for nucleon scattering from nuclei the physical values coincide with half-integer angular momentum numbers. As noted above, in the fixed energy ISP case the S matrix as a function of the angular momentum variable is needed if one is to define uniquely the scattering potential [12].

This equates to knowing the S matrix exactly at all of the infinite set of physical ℓ-values as then the unit step in the quantum number is infinitesimal against the range. Most studies of the fixed energy ISP and notably the Newton-Sabatier (NS) method [6] and its variant, the modified NS method [13], have been applied using only the values of the S matrix specified at a finite set of physical angular momentum values. In real cases, sensible values make that set finite and often quite small in number. Some methods however invoke a functional form for the S function. Specifically the LF methods use one that is identified with Bargmann potentials. In those methods one specifies a set of simple poles and zeroes in the complex angular momentum plane so that the S matrix at the physical (real) angular momenta map to the 'data'. Thus use of a prescription (interpolation/extrapolation) for the S matrix at non-physical values of the angular momentum is not new. However, the LF methods are very prescriptive of the forms of S and are also not without ambiguity in the specification of the function parameters [14]. It suffices that in treating actual scattering problems as fixed energy ISP's, attention must be paid to what S is invoked for non-physical angular momenta.

With the NS and modified NS schemes, such consideration of the S matrix for non-physical ℓ has been done in the past. Münchow and Scheid [13] studied the identical boson scattering problem (^{12}C$-^{12}$C) for which only the even ℓ-partial waves contribute to scattering cross sections. They found some sensitivity in their inversion results according to a choice of the interpolation for odd integer values; most notably of the $\ell = 11$ value for their energy cases. In a recent study of ^{12}C$-^{12}$C scattering however, it was proposed to only use the experimentally available S matrix elements, i.e. at even ℓ-values [29]. Interesting structures were found in the inversion potentials for which physical interpretations were given. In another work, Leeb, Huber, and Apagyi [15] studied the sensitivity of the NS potentials for $n - \alpha$ scattering to selection of the S matrix at non-physical (integer) values of angular momentum interpolated on a physical half-integer value set. They also revisited the ^{12}C-^{12}C scattering problem by adopting a specific Woods-Saxon potential to give the S matrix for all integer l-values. Their limited study showed a sensitivity to the choices of S matrix values

and in this paper we expand upon their results. As no analytic studies on this topic are known to us, we also use the modified NS method as an example for the solution of the ISP at fixed energy.

The NS method is one of the most successful of the fixed energy inversion methods. First numerical tests were carried out by Quyen Van Phu and Coudray [17,18]. Very recently, it has been applied to electron-helium atom scattering [19] using experimental phase shifts of Nesbet [20] at low ℓ-values and dipole polarization phase shifts at higher ℓ-values. Münchow and Scheid [13] modified that approach under the assumption that the potential is known in the region outside the nuclear interaction, i.e. in the infinite interval $(R_{\rm int}, \infty)$. That modified NS method was developed and tested for neutral particle scattering. Later it was extended by May *et al.* [21] to consider charged particles so that the approach became applicable for analysis of experimental data from heavy ion scattering [22–24]. Recently, the method has been extended to facilitate inversion for inelastic scattering [25,26].

In sections II and III the NS and the modified NS methods for the solution of the ISP at fixed energy and elastic scattering will be reviewed in brief. In section IV the optimal choice of the technical inversion parameters $\ell_{\rm max}$ and the Newton radii r_i are specified, the required accuracy of the S matrix elements are studied, and the construction of the potential is investigated in detail. Thus, an optimum solution for the integer-only ISP is found, which is used as a reference in the following sections. In section V the effect of inclusion of non-physical S matrix elements in the inversion procedure is discussed, and we consider how the values of the S matrix at non-physical angular momenta might be obtained. In section VI the results are applied to the experimental differential cross section of the ^{12}C+^{12}C scattering system at $E_{\rm cm} = 7.998$ MeV. Finally, in section VII a summary is made and conclusions are given.

II. THE NS INVERSION METHOD

We consider the elastic scattering of a projectile with mass number A_p and charge number Z_p off a target with mass number A_t and charge number Z_t. The radial Schrödinger equation for this system can be written in the form

$$D^V(r)R^\ell(r) = \ell(\ell+1)R^\ell(r), \tag{1}$$

with the differential operator

$$D^V(r) = r^2\frac{2\mu}{\hbar^2}\left[\frac{\hbar^2}{2\mu}\frac{d^2}{dr^2} + E - V(r)\right], \tag{2}$$

where E is the energy in the center of mass system and μ is the reduced mass and the interaction potential $V(r)$ is the quantity sought. It is presumed that the asymptotic behaviour of the radial wave functions $R^\ell(r)$ is known and has the form:

$$R^\ell(r \to \infty) = A^\ell\left(e^{-i\vartheta_\ell(kr)} - S^\ell e^{i\vartheta_\ell(kr)}\right), \tag{3}$$

where the phase function is given by

$$\vartheta_\ell(kr) = kr - \eta\ln(2kr) - \ell\frac{\pi}{2} + \sigma_\ell, \tag{4}$$

involving

$$\sigma_\ell = arg\Gamma(\ell+1+i\eta), \quad k = \sqrt{\frac{2\mu}{\hbar^2}E}, \quad \eta = \frac{Z_pZ_te^2\mu}{\hbar^2 k}. \tag{5}$$

σ_ℓ are the Coulomb phases, k is the wave number and η is the Sommerfeld parameter. The S matrix elements S^ℓ in Eq. (3) are connected with the phase shifts by $S^\ell = \eta_\ell e^{2i\delta_\ell}$ with values obtained by phase shift analysis of experimental angular differential cross sections or by numerical evaluation of Eq.(1). Such serve as input data for the inversion procedure. The physical S matrix elements are identified by S^ℓ. Later we shall use S matrix elements at non-physical values of the angular momentum and those we shall define by S^λ.

To solve the ISP, one chooses an arbitrary reference potential $V^0(r)$ from which the wave functions $R^{0\ell}(r)$ are known at all radii r and satisfy:

$$D^{V^0}(r)R^{0\ell}(r) = \ell(\ell+1)R^{0\ell}(r). \tag{6}$$

Therein the reference differential operator is

$$D^{V^0}(r) = r^2\frac{2\mu}{\hbar^2}\left[\frac{\hbar^2}{2\mu}\frac{d^2}{dr^2} + E - V^0(r)\right]. \tag{7}$$

With these known reference wave functions, the Povzner-Levitan representation for the solutions of Eq.(1) can be written as [6]:

$$R^\ell(r) = R^{0\ell}(r) - \int_0^r K^{VV^0}(r,r')R^{0\ell}(r')\frac{dr'}{r'^2}. \tag{8}$$

It can be shown [5,6] that Eq.(8) solves the Schrödinger equation Eq.(1) if the integral kernel $K^{VV^0}(r,r')$ fulfills the partial differential equation

$$D^V(r)K^{VV^0}(r,r') = D^{V^0}(r')K^{VV^0}(r,r'), \tag{9}$$

with the boundary conditions

$$K^{VV^0}(r,r'=0) = K^{VV^0}(r=0,r') = 0. \tag{10}$$

The inversion potential then is connected with the kernel by

$$V(r) = V^0(r) - \frac{2}{r}\frac{\hbar^2}{2\mu}\frac{d}{dr}\left[\frac{K^{VV^0}(r,r)}{r}\right]. \tag{11}$$

In the NS method, the integral kernel $K^{VV^0}(r,r')$ is expanded in terms of the wave functions of Eqs.(1) and (6) with some yet unknown spectral coefficients c^ℓ:

$$K^{VV^0}(r,r') = \sum_{\ell=0}^{\infty} c^\ell R^\ell(r)R^{0\ell}(r'), \tag{12}$$

where the sum runs over all integer values of the total angular momentum quantum number $\ell = 0-\infty$. With this kernel, Eq.(8) can be rewritten:

$$R^\ell(r) = R^{0\ell}(r) - \sum_{\ell'=0}^{\infty} R^{\ell'}(r)c^{\ell'}L^{\ell'\ell}(r), \tag{13}$$

where the matrix $L^{\ell'\ell}(r)$ is solely determined by the reference wave functions:

$$L^{\ell'\ell}(r) = \int_0^r R^{0\ell'}(r')R^{0\ell}(r')\frac{dr'}{r'^2}. \tag{14}$$

Eq.(13) is then used in two ways. In a first step the known asymptotic values of the wave functions are used to calculate the spectral coefficients c^ℓ and the normalization coefficients A^ℓ of Eq.(3). It is with this step that the technical parameters, $\ell_{\max}$ and the Newton radii, are required. In a second step, Eq.(13) is then solved to get numerical wave functions $R^\ell(r)$ at discrete radii r_i throughout the interaction volume. With these the potential may then be calculated from Eq.(11) by using Eq.(12).

Newton [27] showed that the set of linear equations Eq.(13) does not have a unique solution. To every energy there exists at least one non zero transparent potential that may add to any solution potential leaving S matrix elements unaltered. However, Sabatier [28] was the first to solve Eq.(13) and give explicit solution vectors. Each of these vectors gives one phase equivalent potential. Under the assumption that the phase shifts tend to zero faster than $\ell^{-3+\varepsilon'}$, Sabatier demonstrated that only one of these potentials decreases asymptotically faster than $r^{-2+\varepsilon}$ (for arbitrary $\varepsilon, \varepsilon'$). All other equivalent potentials show an oscillating tail damped by $r^{-3/2}$ and may be considered as unphysical.

To use the method in numerical calculations, Eq.(13) must be converted into a finite set of equations. This is achieved by truncating the sum at some angular momentum value $\ell_{\max}$. Thus, the potential in the infinite interval $(0, \infty)$ needs to be determined from the finite (and often small) number of phase shifts at angular momentum values of $\ell = 0, ..., \ell_{\max}$. Test calculations using analytic input potentials showed big deviations in results for such inversion potentials [17]. These results were improved by Coudray [18], but only the modification of the method by Münchow and Scheid [13] made feasible application with experimental scattering data as input.

III. THE MODIFIED NS METHOD FOR NEUTRAL PARTICLES

When considering quantum particle scattering, the asymptotic behaviour of the potential is usually known. For the scattering of neutral particles the potential will be zero outside

the nuclear interaction region $r > R_{\rm int}$. Thus the wave functions $R^\ell(r)$ are known in this outer region and are uniquely determined by the S matrix elements as:

$$R^\ell(r > R_{\rm int}) = A^\ell kr T^\ell(r) = A^\ell kr \left[h_\ell^-(kr) - S^\ell h_\ell^+(kr)\right]. \tag{15}$$

Here, $h_\ell^\pm = in_\ell \pm j_\ell(r)$ are the incoming (-) and outgoing (+) spherical Hankel functions, which are formed by irregular and regular spherical Bessel functions. These Bessel functions are solutions of Eq.(1) with $V(r) = 0$; the free Schrödinger equation. As $r \to \infty$ Eq.(15) converges to Eq.(3) with $\eta = 0$.

For neutral particles, the convenient reference potential is zero [13], and the reference solutions are the regular spherical Ricatti-Bessel functions:

$$V^0(r) = 0, \quad R^{0\ell}(r) = kr j_\ell(kr). \tag{16}$$

With Eqs.(15) and (16), the Povzner-Levitan representation Eq.(13) can be reformulated as:

$$A^\ell T^\ell(r) + \sum_{\ell'=0}^{\infty} b^{\ell'} T^{\ell'}(r) L^{\ell'\ell}(r) = j_\ell(kr), \tag{17}$$

where

$$b^\ell = A^\ell c^\ell, \quad L^{\ell'\ell}(r) = \int_0^r j_{\ell'}(kr') j_\ell(kr') \frac{dr'}{r'^2}. \tag{18}$$

By using the assumption $V(r > R_{\rm int}) = 0$, the potential now only needs to be determined in the finite region $0 < r < R_{\rm int}$. Eq.(17) is again solved in two steps. In the first step, two radii (Newton radii) are chosen outside the nuclear interaction region, $r_1, r_2 \geq R_{\rm int}$, to determine the unknown coefficients A^ℓ and b^ℓ. One might consider a choice of more than two Newton radii, thus obtaining an overdetermined set of equations which may be solved by a least squares method. Possible numerical or experimental errors in the input data could be averaged out thereby [22–24].

Once the spectral coefficients are known, Eq.(17) is solved at equidistant radii r_i in the interaction region $0 < r_i < R_{\rm int}$ to give the function $T^\ell(r_i)$. The potential is then obtained from

$$V(r) = -\sum_{\ell} \mathcal{V}^{\ell}(r) = -\sum_{\ell} \frac{2}{r} E b^{\ell} \frac{d}{dr} \left[r T^{\ell}(r) j_{\ell}(kr) \right]. \tag{19}$$

Note also that the case of charged particles can be reduced to the case of neutral particle scattering described in this section by a transformation of the S matrix in the manner discussed in ref. [21].

For numerical calculations again the partial wave sum in Eq.(17) needs to be limited to some finite value $\ell_{\max}$. To date, there is only one superficial numerical study on the effect of this truncation known to the authors, see Ref. [26], and no analytic investigation has been made. It is clear however, that the truncation leaves an incomplete set of functions in which the potential is expanded. This leads to an r-dependency of the spectral coefficients c^{ℓ}. Then the choice of the Newton radii is crucial to the quality of the inversion. In earlier applications of the modified NS method [22–24], $\ell_{\max}$ was determined by the number of available experimental data points $N_{\exp}$ in the phase shift analysis ($4\ell_{\max} + 3 \leq N_{\exp}$; see Ref. [3]), or by the semi-classical estimate $\ell_{\max} \approx kR_{\text{int}}$. For $\ell \gtrsim kR_{\text{int}}$ the centrifugal barrier $\frac{2\mu}{\hbar^2} \frac{\ell(\ell+1)}{{R_{\text{int}}}^2}$ is larger than the energy E.

To include non-physical values of the S matrix in the method, the angular momentum quantum number ℓ is replaced by a rational variable λ. For each value of λ there exists one Schrödinger Eq.(1) and one linear Povzner-Levitan Eq.(17). The NS method is then solved in the same manner described above.

IV. OPTIMAL CHOICE OF THE TECHNICAL PARAMETERS

In this section an optimum solution for the ISP is sought by using S matrix elements specified only at the standard angular momentum quantum numbers $\ell = 0, 1, ...\ell_{\max}$. This optimum solution will then be used as a reference for the calculations made including non-physical values. To get a realistic potential, and an exact S matrix, to test the inversion method numerically, the hypothetical scattering system α+^{12}C at the center of mass energies of $E_{\text{cm}} = 4$ and 50 MeV is considered. This corresponds to wave numbers of $k_4 = 0.78$ fm^{-1} and $k_{50} = 2.63$ fm^{-1} respectively. The analytic optical model potential was chosen to be:

$$V(r) = \frac{V}{e^{(r-R_V)a_V}+1} - i\frac{4W_D e^{(r-R_D)a_D}}{(e^{(r-R_D)a_D}+1)^2} + V_{\text{Coul.}}, \tag{20}$$

$$V_{\text{Coul.}}(r) = \begin{cases} \dfrac{Z_p Z_t e^2}{r} & : \text{ for } r \geq R_{\text{Ch}}, \\ \dfrac{Z_p Z_t e^2}{2R_{\text{Ch}}}\left(3 - \dfrac{r^2}{R_{\text{Ch}}^2}\right) & : \text{ for } r \leq R_{\text{Ch}}, \end{cases} \tag{21}$$

with the parameter values: $V = -15$ MeV, $R_V = 3$ fm, $a_V = 2$ fm^{-1}, $W_D = 7.5$ MeV, $R_D = 2$ fm, $a_D = 3.5$ fm^{-1} and $R_{\text{Ch}} = 3.3$ fm. Although the parameters of this potential have not been determined by fits to experimental cross sections, we note that the chosen values are typical for the scattering system investigated.

The S matrix elements are listed in Table I for $E_{\text{cm}} = 50$ MeV and in Table II for $E_{\text{cm}} = 4$ MeV. They were obtained by numerical integration of Eq.(1) with a stepwidth $\Delta r = 0.01$ fm. The results are specified to 12 decimal places. Such accuracy is taken here to facilitate our investigation of the choice of ℓ_{max} and of the accuracy of input data upon the solution of the ISP, as well as to provide an accurate data set upon which to interpolate. The radius of nuclear interaction, at which the S matrix elements are calculated by matching logarithmic derivatives, was chosen as $R_{\text{int}} = 10.0$ fm. At this distance the real and imaginary parts of the nuclear part of the potential have decreased to be less than 10^{-4} MeV. The S matrix elements are transformed to those of an asymptotic constant potential (as described in ref. [21]) at $r = 10.0$ fm. The S matrix elements converge towards $S^{\ell\to\infty} = 1.0 + i0.0$ and as usual, the higher the energy the more partial waves contribute significantly to the scattering. For the discussion of the optimal choice of the technical parameters we consider only the S matrix elements at $E_{\text{cm}} = 50$ MeV. Qualitatively the results are independent of the scattering energy.

A. The choice of ℓ_{max}

The cut off angular momentum ℓ_{max} must be chosen so that $S^{\ell>\ell_{\text{max}}} = 1.0 + i0.0$ within selected numerical accuracy. Considering that experimental accuracy might be typically $5 - 10\%$, ℓ_{max} should be at least 10 in the example studied here. Hence we solved the ISP

for $\ell_{\max} = 10, 11, 12, ...39$. For those calculations of the unknown coefficients A^ℓ and c^ℓ the two Newton radii $r_1 = 10.0$ fm and $r_2 = 10.01$ fm were chosen. The wave function and the potential were then calculated in the interval (0 fm, 10 fm) with a step width of $\Delta r = 0.01$ fm. As an example for these calculations, the inversion potentials (thick lines) are displayed in Fig. 1 in comparison with the analytic input potentials (thin lines) for cases where the cut off angular momenta are $\ell_{\max} = 15, 16, ...22$, starting from top left and progressing to bottom right. Thus, in the left column all potentials found with odd $\ell_{\max}$ values of 15 to 21 are shown. In the right column the results from using even $\ell_{\max}$ from 16 to 22 are given. From top to bottom the quality of the reproduction generally increases as more and more partial waves are taken into account. However, with these cases the quality of the reproduction depends strongly on whether an even or an odd $\ell_{\max}$ is used. Although 3 more partial waves were taken into account for the inversion potential shown in the second row in the right column compared to the first one shown in the top left diagram, the quality of inversion is poorer. For $\ell_{\max} = 11$ and 13 the inversion potentials (not shown) roughly are the same as the ones shown in Fig. 1 for $\ell_{\max} = 15$ and 17, while the inversion potentials for $\ell_{\max} = 10, 12$ and 14 are distinctly worse than the two potentials displayed for $\ell_{\max} = 16$ and 18. For higher values of $\ell_{\max}$ the inversion potentials remained of the same quality as the one shown for $\ell_{\max} = 22$. The semi-classical estimate would yield $\ell_{\max} \approx 26$. Calculations were carried out up to $\ell_{\max} = 39$. No further improvement of the results could be observed. Indeed the potentials did not change at all. With $S^\ell = 1.0 + i0.0$, the wave functions in the outer region given by Eq.(15) are proportional to the regular spherical Ricatti-Bessel functions, and the $\mathcal{V}^\ell(r)$ vanish.

There are numerical problems with standard methods of solution above and beyond those problems associated with sum truncations, input data accuracy and choice of Newton radii. Such appear from time to time in the form of 'gliches' in potential values. An example is seen in Fig. 1 (right hand panel second from top). In the 8 to 10 fm range little spike effects are evident. The origin and reason for these effects have not been resolved. In all cases though such do not appear in the stabilized, converged results.

To rate the quality of the inversion quantitatively, two χ^2-tests have been performed. The first, χ^2_V, gives the average absolute deviation of the inversion potential from the analytic input one:

$$\chi^2_V = \frac{1}{N}\sum_i \left| \frac{V_{inv}(r_i) - V_{inp}(r_i)}{1MeV} \right|^2, \quad 0.5\,\mathrm{fm} \leq r_i \leq R_{\mathrm{int}} \tag{22}$$

where $V_{inv}(r_i)$ denotes the inversion potential and $V_{inp}(r_i)$ is the analytic input potential. The summation starts at $r = 0.5$ fm thus excluding the pole at $r = 0$ fm; the origins of which will be discussed later. The total number of points was $N = 950$. The second, χ^2_S, involves the S matrix elements:

$$\chi^2_S = \frac{1}{\ell_{\max}} \sum_{\ell=0}^{\ell_{\max}} \left| S^\ell_{inv} - S^\ell_{inp} \right|^2 . \tag{23}$$

This gives the average absolute deviation of the inversion S matrix elements S^ℓ_{inv} (as calculated from the inversion potential by integration of the Schrödinger equation) from the input S matrix. While χ^2_S-test can always be performed for the inversion S matrix, χ^2_V is only available for analytic examples where the input potential is known.

In Fig. 2 χ^2_V and χ^2_S are shown semi-logarithmically as functions of $\ell_{\max}$ for $\ell_{\max} = 10-30$. The lines are simply to guide the eye. For even higher $\ell_{\max}$ (up to 39) the χ^2-values remained stable. For $\ell_{\max} < 15$ the even-odd dependency of the inversion potentials can be seen clearly, with the effect remaining visible to $\ell_{\max} = 20$. For $\ell_{\max} > 22$ the χ^2-values have reached their minimum and remain stable. The progression of χ^2_S reflects the quality of the inversion potential as rated by χ^2_V. However, even the comparatively bad inversion potentials from use of $\ell_{\max} = 15, 16, 17$, and 18 (shown in the upper half of Fig. 1) which have a χ^2_V of about 100, the reproduction of the S matrix is fairly good ($\chi^2_S \approx 10^{-5}$).

For $\ell_{\max} = 22$ the values are $\chi^2_V = 0.02$ and $\chi^2_S = 2.5810^{-10}$. The differences between the real- and imaginary parts of the S matrix elements are shown in Table III. On average this difference is significantly smaller than 0.01%. The rise of the difference for the imaginary part at larger values of ℓ is due to the fact that the absolute values approach the numerical zero (see Table I). The slightly larger deviation of the s-wave S matrix element is an effect of the pole at $r = 0$.

Clearly it is possible to determine an optimum value for $\ell_{\max}$, which in the example discussed here is $\ell_{\max} = 22$. This means also that the numerical accuracy required by the inversion procedure of the input S matrix (see $S^{\ell=22}$ in Table I) is at least 5 digits.

B. The required accuracy of the S matrix elements

To study this aspect further, we simulate an experimental error by simply cutting off decimal digits of the given S matrix elements. In Fig. 3 the result of these calculations are presented. The thin curves correspond to the optimum inversion potential for $\ell_{\max} = 22$ using the set of S matrix elements as given in Table I. The results displayed by the thick curves were obtained by limiting the number of decimal digits of the S matrix used in the inversion to 2,3,4, and 5. These results are given in this figure reading from top to bottom. For 6 digits the accuracy of the optimum potential is achieved. The value for $\ell_{\max}$ in these calculations was adjusted to the values for which the S matrix is $1.0 + i0.0$ within the accuracy. The corresponding values are $\ell_{\max} = 15$, 18, 20, and 22 (see Table I). We have also calculated the χ^2 values and for the 2,3,4, and 5 digit accuracy cases they are: $\chi^2_V = 75.34, 184.16, 1.53$ and 0.02; $\chi^2_S = 1.0710^{-3}, 1.0310^{-2}, 3.1310^{-3}$ and 3.7110^{-7}. Even though the inversion potential for which 5 digits of the S matrix have been used already has the same quality as the optimum result $\chi^2_V = 0.02$, the reproduction of the S matrix is still 3 orders of magnitude worse. This shows that the S matrix-elements need to be known with very high precision in order to get reliable results. A minimum of 5 digits should be used. This is also reflected by the value of $\chi^2_S \propto 10^{-10}$ for the optimum result. On average, the input S matrix is reproduced exactly up to 5 digits.

C. The choice of the Newton radii

In this subsection we consider the effect of the relative distance, the absolute distance from the radius of nuclear interaction R_{int}, and the number of Newton radii on the quality of inversion. For these studies the value of the cut off angular momentum was fixed at

$\ell_{\max} = 22$. Results are compared to the optimum inversion potential found in subsection IV A for $\ell_{\max} = 22$, $r_1 = 10$ fm and $r_2 = 10.01$ fm (thin lines in the Figures).

The left panel of Fig. 4 shows the inversion potentials for different relative distances of two Newton radii, the first of which is fixed at $r_1 = 10.0$ fm. The results shown in that panel from top to bottom were found when the second radius r_2 was taken to be 11.0 fm, 12.0 fm, and 13.0 fm. While the result in the top diagram has approximately the quality of the optimum solution ($\chi_V^2 = 0.06, \chi_S^2 = 2.3910^{-6}$), the other two with $\Delta r = 2.0$ fm ($\chi_V^2 = 0.33, \chi_S^2 = 6.310^{-3}$) and $\Delta r = 3.0$ fm ($\chi_V^2 = 19.01, \chi_S^2 = 1.18$) do not.

The center panel in Fig. 4 shows the inversion potentials for different absolute distances from the radius of nuclear interaction R_{int}, while keeping the relative distance constant at $\Delta r = 0.01$ fm. The results shown from top to bottom coincide with the first Newton radius r_1 being 11.0 fm ($\chi_V^2 = 0.33, \chi_S^2 = 5.1810^{-5}$), 12.0 fm ($\chi_V^2 = 2.26, \chi_S^2 = 3.7610^{-3}$), and 13.0 fm ($\chi_V^2 = 50.33, \chi_S^2 = 2.7310^{-3}$). Again, only the first example compares adequately with the optimum solution.

The right panel of Fig. 4 contains the inversion potentials found on using different numbers of Newton radii. For more than two Newton radii Eq. (17) becomes an overdetermined set of equations. That has been solved by a least squares method to specify the optimum solution. The relative distance between the radii was fixed at $\Delta r = 0.01$ fm. The number of Newton radii are: 3 ($\chi_V^2 = 0.05, \chi_S^2 = 1.1710^{-7}$), 4 ($\chi_V^2 = 0.05, \chi_S^2 = 7.6610^{-10}$), and 5 ($\chi_V^2 = 0.05, \chi_S^2 = 7.3610^{-10}$), with $r_1 = 10.0$ fm respectively for the figures shown in the top, middle and bottom frame. None of these is an improvement on the original result which used just two Newton radii.

It can be concluded that the Newton radii need to be chosen near to the radius of nuclear interaction (commensurate with the matching radius for specification of the S matrix elements in this test case), and that the relative distance between them should be small. For the highly accurate input data used in these calculations, while the number of Newton radii chosen does not improve the results, the results depend strongly on the choice of $\ell_{\max}$. Similar calculations with $\ell_{\max} = 21$ (not presented here) showed a much stronger

dependency of the inversion potentials on the choice of the Newton radii. The r-dependency of the spectral coefficients c^ℓ can be minimized only if a large enough number of S matrix elements are used in the inversion procedure.

D. The construction of the potential from the kernel

With numerical requirements of the inversion method established, we now examine how the potential is composed by a study of the contributions of the different $\mathcal{V}^\ell(r)$ in the sum in Eq.(19). In Fig. 5 the first 10 individual terms $\mathcal{V}^\ell(r)$ of the optimum solution found in subsection IV A (for $\ell = 0, 1...9$) are displayed. The partial wave value of each increases as one proceeds downwards from top left to bottom right. The real and imaginary parts are displayed by the continuous and dashed curves respectively. Save for the $\ell = 0$ contribution, all terms are regular at the origin. The pole in $V(r)$ at $r = 0$ is caused exclusively by the term $\mathcal{V}^{\ell=0}(r)$. We also note that the pole at $r = 0$ is inherent to the NS method. It is not caused by the truncation of the partial waves and so it can not be removed by taking additional S matrix elements into account.

For small values of ℓ and large radii, $\mathcal{V}^\ell(r)$ is very small. When ℓ approaches $\ell_{\max}$, the contribution of $\mathcal{V}^\ell(r)$ at small radii is negligible. Thus for a given interval $[r_1, r_2]$ the potential is almost completely determined by the contributions from a limited number of ℓ values $(\ell_1, \ell_2) \in (0, \ell_{\max})$. To demonstrate this, we show in Fig. 6 how the potential is build up from the inside out by adding $\mathcal{V}^\ell(r)$ for increasing cut off limits in the sum. From top left to bottom right the first 2,3,...,10 terms of the sum in Eq.(19) are taken into account. In the last diagram (with 11 terms summed), the potential is already fully determined for the region (0 fm,2.5 fm). It can be concluded then, that the total number of terms one need take in the summation of the kernel needs to be large enough to allow a reasonable coverage of the whole radial interval for which the potential is sought.

However, there is another condition that indicates possible problems for low energy (few partial wave sensitive) results. For a small region around any chosen point r, only a few

partial wave terms $\mathcal{V}^{\ell}(r)$ seriously contribute in the sum Eq.(19). How many depends on the relative wave number (energy). This (limited) sums of oscillating functions may not have converged sufficiently if only a few entries are involved and one can expect an oscillatory result for $V(r)$ and possibly strongly so. Essentially this indicates that the chosen ($\Delta\lambda = 1$) gap in the tabulation, physical values though they be, is too large in comparision to the defined range of S^{ℓ} elements. The infinite sum for $\ell_{\max} - \infty$ of numerically very small terms restricted to just physical ℓ values may need to be included to offset such spurious effects in principle. This leads us to consider use of inversion with S^{λ} sets where λ includes non-integer values of angular momentum quantum numbers, thus providing additional functional space in the expansion of the integral kernel.

V. INCLUSION OF NON-INTEGER VALUED PARTIAL WAVES

Seeking increase in the quality of reproduction of the input potential, we now consider the inclusion of non-integer valued partial waves in the expansion of the integral kernel Eq.(12) as was proposed in Ref. [15]. In a first application, the half, quarter, and eighth integer values of the S^{λ} matrix elements at $E_{\rm cm} = 50$ MeV were calculated by solving the relevant Schrödinger equation Eq.(1) with the Woods-Saxon potential. The enlarged sets of S matrix elements were then used in the inversion procedure. The technical parameters chosen in those calculations were the optimum values found previously. The resulting potentials are shown in the left panel of Fig. 7 by thick solid and dashed curves for the real and imaginary parts respectively. They are compared with the optimum result (with $\Delta\lambda = 1$) found previously. From top to bottom the number of S matrix elements taken as input were doubled in each calculation as half-, quarter and finally eighth partial waves enter the sum in Eq.(12). In this case the inversion potentials all have approximately the same quality as the optimum result we obtained from inversion specified by S^{λ} for integer values of λ. The χ^2-values are (from top to bottom): $\chi^2_V = 0.03, 0.04$ and 0.14. For the $\Delta\lambda = 0.5$ calculation $\chi^2_S = 6.8010^{-10}$. To facilitate study of the $\Delta\lambda = 0.25$ and 0.125 cases and to avoid numerical problems arising

from the calculation of the Coulomb functions at small stepsizes both in radii and angular momentum, the stepsize of the inversion potentials was increased to $\Delta r = 0.1$ fm. As the accuracy of the S matrix elements depends on that step width in integration of the ensuing Schrödinger equations, the χ^2_S-values should not be compared to the earlier results. For the $\Delta\lambda = 0.25$ and 0.125 calculations however χ^2_S is still about 10^{-7}.

For even smaller stepsize of the angular momentum, the results should become stable in principle, but numerical inaccuracies in the calculation of the wavefunctions at the rational angular momenta values in some cases gave rise to numerical noise. Nevertheless, the important feature in this case is that the information available from the integer-only S matrix elements is already sufficient to determine the potential.

However, when a lesser number of partial waves contribute sensibly to the scattering, inclusion of non-physical values in the S matrix in the inversion theorem might reveal additional information on the underlying interaction. As an example, we consider the given scattering system at the energy of $E_{\rm cm} = 4$ MeV. This energy is about 1 MeV above the Coulomb barrier. Only 6 partial waves are not $1 + i0$ within the required precision (see Table II). The inversion potential for this S matrix (with $\Delta\lambda = 1$) is displayed by the thick solid (real) and dashed (imaginary) curves in the top diagram of the right hand panel of Fig. 7. In comparision with the analytic input potential, the reproduction is very poor ($\chi^2_V = 11.8, \chi^2_S = 0.1410^{-4}$). The diagram in the centre of the right hand panel of Fig. 7 shows the inversion potential found when half integer values of the S matrix were included. In this case $\chi^2_V = 0.28$ and $\chi^2_S = 0.3310^{-5}$. The bottom segment displays the results of inversion on using quarter integer values ($\chi^2_V = 0.23, \chi^2_S = 0.4910^{-5}$). The basic result in the top diagram is significantly changed and for the better by the inclusion of the non-physical S^λ values in the inversion process. Smaller stepsizes of $\Delta\lambda$ only marginally improved the quality of result we have here.

In the examples discussed, the input S matrix for all values of angular momentum (including rational ones) was found by numerical evaluation of the Schrödinger equation, Eq.(1). Thereby the input data for these inversion studies could be calculated with high

precision. When applying the inversion method to experimental scattering data however, only the S matrix values for physical (integer valued) partial waves can be derived. Only the even ℓ-values can be in the case of identical boson scattering. Thus to improve the inversion by inclusion of half integer values in the set, an interpolation of the known S matrix elements needs be made. As a test, we consider the S matrix elements as given in Tables I and II for integer values $\lambda = \ell$, and try to deduce the values of half integer λ without solving the Schrödinger equation.

To do so the integer values for $\ell = 0, 1, 2, ..., 22$ of the S matrix elements at $E_{\rm cm} = 50$ MeV (Table I) were fit using a rational form for the S matrix (Bargmann scheme [7]) as has been proposed in Ref. [15]. This rational form was then used to specify the S matrix elements at half integer λ. Thus, a physically motivated interpolation for the S matrix has been used. The tabled integer λ S matrix elements were fit with a precision of 10^{-6} per datapoint, thereby achieving the accuracy of input as deemed necessary from the studies reported in subsection IV B. In Fig. 8, the interpolated S matrix elements are compared to the exact ones in the Argand diagram. The exact (integer λ) values are shown as stars and the exact values at half integer λ are given by the crosses. They are connected by dashed lines solely to guide the eye. The interpolated values are represented by circles and again to guide the eye are connected by full lines. The S matrix element with $\ell = 0$ is that at the lower left end of the curve formed by the set. We stress that the lines are neither interpolations nor do they give the exact devolution of the S matrix elements to other rational values of angular momentum. As ℓ approaches $\ell_{\rm max}$, the elements move closer to the point $1.0 + i0.0$. All but the first two S matrix elements of half integer λ are reproduced very well by the interpolation, although the rational form of the S matrix has only been fit to the values at integer λ. These interpolated values together with the exact integer values then serve as input to the inversion procedure. The resulting inversion potential (using two Newton radii $r_1 = 10.0$ fm and $r_2 = 10.01$ fm) is shown in the top diagram of Fig. 9. The relatively small deviations of the interpolated values from the exact values give rise to huge oscillations and severe numerical problems at larger radii. The input potential is not reproduced; an effect

reflected in the χ^2 values $\chi^2_V = 62.06$ and $\chi^2_S = 8.110^{-3}$. To try to average out the numerical errors of the interpolated set of S matrix elements, the least-squares method as described in subsection IV C was used. The best result was obtained for three equidistant Newton radii with $r_1 = 10.0$ fm and $\Delta r = 0.01$ fm, and that is shown in the bottom diagram of Fig. 9. For this result $\chi^2_V = 26.64, \chi^2_S = 7.610^{-6}$. While the inversion potential so found now oscillates around the input one there has been no improvement over the integer-only-values optimum result discussed in subsection IV A.

We now consider the lower energy case at $E_{\rm cm} = 4$ MeV for which the inversion potential was actually improved by the inclusion of analytic S^λ of half integer λ. In Fig.10 the interpolated values of the S matrix are compared to the exact ones in the Argand diagram. In the top and middle segments the 7 S matrix elements given in Table II are shown as stars. This would be the input data under the choice that such are taken solely from the experiment. One is now faced with the problem of finding a reasonable and proper interpolation for this set. Again we used a fit with a rational form of the S matrix with a precision of 10^{-6} per base S matrix element. The interpolation (full curve) together with the values at half integer λ (circles) is shown in the center diagram of Fig. 10. Although the rational form again fits with high accuracy, the interpolated values at half integer λ do not coincide with the exact ones we obtained from the solution of the Schrödinger equation. This is evident in the diagram at the bottom of the figure where the exact (calculated) S matrix values are shown by + signs, and the exact (calculated) progression is shown by the dashed line. To find these exact values by an interpolation on the limited set of S matrix elements one can extract from 'data' i.e. the physical set at integer values of λ (as shown in the top diagram) one must have more information about the interaction. Without this additional information, a successful interpolation of the set of integer S matrix elements seems impossible. In Fig. 11 we show the inversion potentials calculated with the interpolated set of S matrix elements and calculated with two different sets of Newton radii. Neither of the two results reproduces the input potential and neither improves upon the integer-only inversion potential. Given that the analytic potential gave such a different calculated S function that result is not surprising.

Only the asymptotic properties of the potential are reproduced correctly as these are mainly determined by the large angular momenta, which are interpolated reasonably well by this prescription.

VI. SCATTERING OF IDENTICAL PARTICLES

As an application in a physical case, i.e. using actual data, we consider the scattering of two ^{12}C-nuclei at an energy of $E_{\rm cm} = 7.998$ MeV. Due to the indistinguishability of projectile and target, the differential cross section is symmetric about 90° in the center of mass as only the S matrix elements for even partial waves contribute to the cross section. S matrix elements of odd partial waves can only be obtained by an interpolation of those physical even-ℓ S matrix values.

Much ^{12}C+^{12}C scattering data has been obtained by Voit and co-workers [22] and many analyses of that data have been made during the last 10 years [22,23,29]. Recently, a new ansatz within the modified NS formalism was proposed using only the physical S matrix elements (of the even partial waves) to invert this data [29]. As this ansatz is closely related to the matters we have discussed in this paper, we assess this interesting proposal by using properties of a fitted analytic potential, as again such provides us with the 'correct' S^λ for all λ.

The cross section data for ^{12}C+^{12}C scattering at $E_{\rm cm} = 7.998$ MeV is shown as the ratio to Rutherford in Fig. 12 and therein it is compared with a fit (solid curve) obtained with a Woods-Saxon optical model potential whose potential parameters are:

$$\begin{aligned} V &= -16.3\text{MeV}, R_V = 5.51\text{fm}, a_V = 0.98\text{fm}^{-1} \\ W_D &= 12.55\text{MeV}, R_D = 3.27\text{fm}, a_D = 7.54\text{fm}^{-1} \\ R_{\rm Ch} &= 5.69\text{fm} \end{aligned} \tag{24}$$

The fit found using this potential gives a $\chi^2 = 37.6$ per data point. Better fits might be obtainable, but we are only interested in having a defined realistic potential for our discussion

and not in an optimal explanation of the scattering data. As the scattering energy is just 2.5 MeV above the Coulomb barrier this system is comparable to the low energy analytic example we investigated previously.

From experimental data only the S matrix elements for even partial waves can be extracted. But from the given fitted potential we can specify the values of S matrix elements at all partial waves by numerical evaluation of the Schrödinger equation. In a first inversion calculation we used only the S matrix elements at even partial waves ($\Delta\ell = 2$) as was proposed in Ref. [29], in a second we used the more complete set which has $\Delta\ell = 1$. The two results of those inversions are compared in the top and bottom segments of Fig. 13 respectively to the fitted analytic input potential. Neither reproduce the Woods Saxon potential from which the S matrix elements were defined. The inversion potential for which only the physical values have been used (the $\Delta\ell = 2$ case) does not reproduce even the basic features of the input potential. Note that this $\Delta\ell = 2$ potential shows the same behaviour as the potential shown in Ref. [29]. The inversion potential found using the more complete set of S matrix elements (the $\Delta\ell = 1$ case) also is a poor reproduction. However, it oscillates around the original potential.

The inversion S matrix elements are compared to the input ones for the two potentials in the Argand diagram given in Fig. 14. The exact values are shown by the crosses, the inversion S matrix elements are displayed by the circles. Both potentials reproduce the input S matrix elements within the accuracy of experimental input data (roughly 5%). As two times more information is used to construct the $\Delta\ell = 1$ potential, it is clear that the reproduction (shown in the bottom segment of Fig. 14) is significantly better. We also note that, as in the low energy example discussed in subsection V, the values of the S matrix elements at non-integer angular momentum can not be calculated by a simple mathematical interpolation. The full line gives the calculated (Woods-Saxon potential) progression of the S matrix elements. The imaginary part of that S matrix changes sign 4 times; a feature that to us seems impossible to find by interpolation on the 7 values ($\times$) shown in the top diagram.

Clearly here is a case, physically motivated that can be solved only by having far more information about the functional dependence of the S matrix than can be deduced from the fixed energy scattering data alone.

VII. SUMMARY AND CONCLUSIONS

In this paper the question of whether the process of inversion of fixed energy data can be improved by including non-physical S matrix elements has been discussed.

First, we found an optimum solution for a given optical model potential based upon the modified NS inversion method. The utilized inversion method inherently has a pole at the origin which can not be removed by increasing the technical parameter $\ell_{\max}$ or a good choice of the Newton radii. Nonetheless a stable result can be derived that reproduces the input data with high accuracy. We have found that the Newton radii need to be chosen very close to each other, and as close to the radius of nuclear interaction as possible. Solving an overdetermined set of equations by means of a least squares method improved the results but only if the input data was inexact. However, the required accuracy of the S matrix elements has been shown to be 5 decimal digits - a precision unlikely to be achieved even in principle from experimental data.

The inclusion of non-physical S matrix elements (for non integer λ) does improve the inversion in cases where very few partial waves contribute to the scattering. We conclude that $\Delta\lambda$ should be small compared to $\lambda_{\max}$ to guarantee a fair reproduction of the interaction potential.

The results have been applied to the well studied symmetric scattering system of $^{12}C+^{12}C$ at a low energy. It was found that to determine the interaction potential non-physical S matrix elements must be used in the inversion process. Restricting inversion to be based upon physical values only we find potentials very similar to those published [29] but, given our controlled study, clearly the process lacks input information. The results are not reliable as a physical prescription.

Leeb *et al.* [15] proposed the inclusion of interpolated non-integer partial waves in the inversion of low energy $^{12}C+^{12}C$ scattering. As we have shown in this paper, it may be impossible to find a physically motivated interpolation to determine those non-physical S matrix elements and certainly so within the required accuracy. In Ref. [15], it was noted that small changes in the non-physical S matrix elements have a major effect on the inversion potentials. We also find that to be so. Therefore we conclude that the inclusion of non-physical partial waves in the inversion procedure can only improve the inversion potential if the additional S matrix elements can be obtained with high accuracy (5 decimal digits), such as from the direct solution of the Schrödinger equation. For low energy scattering there seems to be insufficient information to date to consider the resultant inversion potentials as reliable physical ones and for higher energy scattering one needs to consider the vagaries that can arise due to the limitations of the accuracy that existing data can specify for the S^ℓ matrix elements.

We believe that *a priori* information about the interaction systems need be used in conjunction with the conventional global inverse scattering theory studies if the results are to be a proper representation of the interaction potentials. The question remains, where this *a priori* information can come from and how it should be implemented in the inversion procedure. Further studies in this direction are needed.

Acknowledgments: One of the authors (ME) gratefully acknowledges the support of an Australian Research Council Postdoctoral Fellowship. The authors are thankful to Prof. Les Allen for many stimulating discussions.

REFERENCES

[1] W. Tiereth, Z. Basrak, N. Bischof, H. Fröhlich, and H. Voit, Nucl. Phys. **A 440**, 143 (1985); D.R. Lun, L.J. Allen, and K. Amos, Phys. Rev. A **50**, 4000 (1994); V. Chisté, R. Lichtenthäler, A.C.C. Villari, and L.C. Gomes, Phys. Rev. C **54**, 784 (1996).

[2] M. T. Bennett, C. E. Steward, K. Amos, and L. J. Allen, Phys. Rev. C **54**, 822 (1996).

[3] C. Marty, Lecture Notes in Physics **156**, 216 (1982).

[4] H. Huber, D. R. Lun, L. J. Allen, and K. Amos, Phys Rev. A **55**, 2015 (1997).

[5] R.G. Newton, *Scattering of Waves and Particles*, 2nd edition, Springer-Verlag, New York, (1982).

[6] K. Chadan and P.C. Sabatier, *Inverse Problems in Quantum Scattering Theory*, 2nd edition, Springer-Verlag, New York, (1989).

[7] R. Lipperheide and H. Fiedeldey, Z. Phys. A **286**, 45 (1978); *ibid.* A**301**, 81 (1981).

[8] M.A. Hooshyar and M. Razavy, Canad. J. Phys., **59**, 1627 (1981).

[9] W.A. Schnizer and H. Leeb, J. Phys. **A26**, 5145 (1993); *ibid.* **A27**, 2605 (1994).

[10] H. Huber and H. Leeb, Eur. Phys. J. **A1**, 221 (1998); J. Phys. **G24**, 1287 (1998).

[11] D.R. Lun and S.J. Buckman, Phys. Rev. Lett. **79**, 541 (1997); D.R. Lun, M. Eberspächer, K. Amos, W. Scheid, and S.J. Buckman, Phys. Rev. A **58**, 4993 (1998).

[12] J. J. Loeffel, Ann. Inst. Henri Poincare **8**, 339 (1968).

[13] M. Münchow and W. Scheid, Phys. Rev. Lett. **44**, 1299 (1980).

[14] L. J. Allen, K. Amos, and P. J. Dortmans, Phys. Rev. C **49**, 2177 (1994).

[15] H. Leeb, H. Huber, and B. Apagyi, in *Inverse and Algebraic Quantum Scattering Theory*, edited by B. Apagyi, G. Endrédi, and P. Lévay, LNP 488 (Springer Verlag, Berlin, 1997), pp. 75-87.

[16] R.G. Newton, J. Math. Phys. **3**, 75 (1966); P.C. Sabatier, *ibid.* **7**, 1515 (1966).

[17] P.C. Sabatier and F. Quyen Van Phu, Phys. Rev. D **4**, 127 (1971).

[18] C. Coudray, Lett. Nuovo Cim. **19**, 319 (1977).

[19] Z. Harman, *Elektron-hélium ütközés effektív kölcsönhatásának meghatározása kísérleti szórásadatokból*, Scientific Student Work, Technical University of Budapest, Budapest, 1999 unpublished.

[20] R. K. Nesbet, J. Phys. **B12**, L243 (1979); Phys. Rev. A **20**, 58 (1979).

[21] K.E. May, M. Münchow, and W. Scheid, Phys. Lett. **B141**, 1 (1984).

[22] B. Apagyi, A. Ostrowski, W. Scheid, and H. Voit, J. Phys. **G18**, 195 (1992).

[23] A. Schmidt, *Verbindung von Phasenanalyse und Inversem Streuproblem bei fester Energie und Anwendung auf die elastische* ^{12}C+^{12}C*-Streuung*, diploma thesis, Justus-Liebig-Universität Gießen (1992), unpublished; B. Apagyi, A. Schmidt, W. Scheid, and H. Voit, Phys. Rev. C **49**, 2608 (1994).

[24] B. Apagyi, K. Ladány, P. Lévay, and I. Nagy, Periodica Polytechnica Ser. Phys. and Nucl. Sci. **1**, 225 (1993); B. Apagyi, P. Lévay, and W. Scheid, in *Inverse and Algebraic Quantum Scattering Theory*, edited by B. Apagyi, G. Endrédi, and P. Lévay, LNP 488 (Springer Verlag, Berlin, 1997), pp. 158-168; N. Alexander, K. Amos, B. Apagyi, and D.R. Lun, Phys. Rev. C **53**, 88 (1996).

[25] M. Eberspächer, B. Apagyi, and W. Scheid, Phys. Rev. Lett. **77**, 1921 (1996); M. Eberspächer, B. Apagyi, and W. Scheid, Revista Mexicana de Fisica **43**, 14 (1997); M. Eberspächer and W. Scheid, J. Math. Phys. **39**, 3061 (1998); M. Eberspächer, K. Amos, W. Scheid, and B. Apagyi J. Math. Phys. submitted 1999.

[26] M. Eberspächer, B. Apagyi, and W. Scheid, in *Inverse and Algebraic Quantum Scattering Theory*, edited by B. Apagyi, G. Endrédi, and P. Lévay, LNP 488 (Springer Verlag,

Berlin, 1997), pp. 98-111.

[27] R.G. Newton, J. Math. Phys. **3**, 75 (1966).

[28] P.C. Sabatier, J. Math. Phys. **7**, 1515 (1966).

[29] B.Apagyi, G. Endrédi, and P. Lévay, Heavy Ion Physics **5**, 167 (1997).

ℓ	$Re(S^\ell)$	$Im(S^\ell)$	ℓ	$Re(S^\ell)$	$Im(S^\ell)$
0	-.28659 38716 99	-.59145 23953 06	20	.99999 99677 52	.00017 03125 80
1	-.60638 12597 30	-.14367 49326 00	21	.99999 99911 73	.00008 38484 96
2	-.61077 40878 71	.17635 93766 74	22	.99999 99975 74	.00004 09312 91
3	-.44421 91441 45	.31336 06161 58	23	.99999 99993 37	.00001 94599 18
4	-.26111 02822 98	.39612 04474 75	24	.99999 99998 21	.00000 88093 28
5	-.08957 83725 33	.54065 22005 73	25	.99999 99999 52	.00000 37226 80
6	.15132 90308 47	.69323 36192 57	26	.99999 99999 87	.00000 14490 82
7	.49340 49404 93	.70839 26237 75	27	.99999 99999 97	.00000 05159 64
8	.78666 53275 80	.53680 03734 86	28	.99999 99999 99	.00000 01676 49
9	.93085 99057 32	.32564 98005 30	29	1.00000 00000 00	.00000 00497 33
10	.98038 98487 49	.17685 47697 85	30	1.00000 00000 00	.00000 00134 98
11	.99474 69566 53	.09161 11634 92	31	1.00000 00000 00	.00000 00033 61
12	.99862 47954 05	.04647 05553 76	32	1.00000 00000 00	.00000 00007 70
13	.99964 28002 13	.02332 77788 96	33	1.00000 00000 00	.00000 00001 63
14	.99990 72769 54	.01164 11736 56	34	1.00000 00000 00	.00000 00000 32
15	.99997 58519 87	.00578 73076 63	35	1.00000 00000 00	.00000 00000 06
16	.99999 36747 27	.00286 97762 30	36	1.00000 00000 00	.00000 00000 01
17	.99999 83310 75	.00142 02792 28	37	1.00000 00000 00	.00000 00000 00
18	.99999 95562 25	.00070 14315 82	38	1.00000 00000 00	.00000 00000 00
19	.99999 98809 89	.00034 57260 07	39	1.00000 00000 00	.00000 00000 00

TABLE I. Real and imaginary part of the S^ℓ matrix elements found from the optical potential calculation of 50 MeV α+^{12}C scattering.

ℓ	$Re(S^\ell)$	$Im(S^\ell)$
0	.62542 13542 72	.22774 90013 38
1	.66111 42953 85	-.04146 21246 65
2	.92176 03347 71	.13966 78075 26
3	.99823 03127 70	.01953 70795 29
4	.99994 35492 53	.00254 32356 11
5	.99999 78851 26	.00032 66906 88
6	.99999 99138 31	.00004 04275 74

TABLE II. Real and imaginary part of the S^ℓ matrix elements found from the optical potential calculation of 4 MeV α+^{12}C scattering.

ℓ	$\frac{Re(S^\ell_{inv}-S^\ell_{inp})}{Re(S^\ell_{inp})}$[%]	$\frac{Im(S^\ell_{inv}-S^\ell_{inp})}{Im(S^\ell_{inp})}$[%]	ℓ	$\frac{Re(S^\ell_{inv}-S^\ell_{inp})}{Re(S^\ell_{inp})}$[%]	$\frac{Im(S^\ell_{inv}-S^\ell_{inp})}{Im(S^\ell_{inp})}$[%]
0	0.004860	0.011270	12	-0.000023	-0.007113
1	-0.000086	-0.004292	13	0.000006	-0.005682
2	0.003384	0.005530	14	-0.000184	-0.015499
3	0.001831	-0.001019	15	-0.000177	-0.027412
4	-0.001398	-0.004180	16	0.000001	-0.014780
5	0.000872	-0.001977	17	0.000018	-0.075586
6	-0.003830	0.000218	18	-0.000059	-0.340952
7	0.000115	0.000853	19	-0.000053	-0.526721
8	0.000702	-0.000220	20	0.000004	-0.204275
9	0.000462	-0.002056	21	0.000013	-0.238560
10	0.000151	-0.002976	22	-0.000029	-3.314516
11	0.000073	-0.005600			

TABLE III. Percentage variance between the input S^ℓ elements and those extracted by using the inversion potential.

Figure captions

Figure 1. Inversion potentials (real part: thick solid curve; imaginary part: thick dashed curve) in comparison with analytic input potential (real part: thin solid curve; imaginary part: thin dashed curve) for $\ell_{\max} = 15, 16, ..., 22$, presented row-wise from top left to bottom right

Figure 2. χ^2_V (upper figure) and χ^2_S (lower figure) as functions of $\ell_{\max}$.

Figure 3. Inversion potentials obtained by using increasingly accurate input data (real part: thick solid curve; imaginary part: thick dashed curve) compared to the optimum result (real part: thin solid curve; imaginary part: thin dashed curve).

Figure 4. Inversion potentials obtained for different sets of Newton radii (real part: thick solid curve; imaginary part: thick dashed curve) as compared to the optimum result (real part: thin solid curve; imaginary part: thin dashed curve). In the left panel the effect of varying relative distance between two Newton radii is shown. In the center panel, the results of varying absolute distance from the nuclear interaction region are presented. The effects of varying the number of Newton radii used are displayed in the right panel.

Figure 5. Individual contributions of the terms $\mathcal{V}^\ell(r)$ of the kernel to the potential for $\ell = 0 - 4$ (from top to bottom, left column) and $\ell = 5 - 9$ (top to bottom, right column). The real and imaginary parts are displayed by the continuous and dashed lines respectively.

Figure 6. Partial summation over the terms $\mathcal{V}^\ell(r)$ from $\ell = 0$ to $\ell = 1 - 5$ (from top to bottom; left column) and from $\ell = 0$ to $\ell = 6 - 10$ (from top to bottom; right column). The real and imaginary parts are given by the solid and dashed curves respectively.

Figure 7. Inversion potentials obtained by inclusion of non integer valued partial waves (real part: thick solid curve; imaginary part: thick dashed curve) as compared to the optimum result (real part: thin solid curve; imaginary part: thin dashed curve) at $E_{\rm cm} = 50$ MeV (left column) and $E_{\rm cm} = 4$ MeV (right column). From top to bottom, left column: $\Delta\lambda = \frac{1}{2}$, $\Delta\lambda = \frac{1}{4}$, and $\Delta\lambda = \frac{1}{8}$. From top to bottom, right column: $\Delta\lambda = 1$, $\Delta\lambda = \frac{1}{2}$, and $\Delta\lambda = \frac{1}{4}$.

Figure 8. Exact and interpolated S matrix elements in the Argand diagram for $E = 50$ MeV. Exact S matrix values coinciding with integer values of the angular momentum variable (λ) are shown as stars, exact values calculated at half integer values are shown as '+' and to guide the eye are connected by the dashed line. The interpolated values at half-integer λ are shown by circles and are connected with the full line.

Figure 9. Inversion potentials obtained using the interpolated set of S matrix elements (real part: thick solid curve; imaginary part: thick dashed curve) compared with the analytic input potential (real part: thin solid curve; imaginary part: thin dashed curve).

Figure 10. Exact and interpolated S matrix elements in the Argand diagram for $E = 50$ MeV. Exact S matrix values defined at integer values of the angular momentum λ are shown as stars, exact values calculated at half integer values of λ are shown by the '+' and are connected by the dashed line. The interpolated values are shown by circles and are connected with the full line.

Figure 11. Inversion potentials obtained from the interpolated set of S matrix elements (real part: thick solid curve; imaginary part: thick dashed curve) compared with the analytic input potential (real part: thin solid curve; imaginary part: thin dashed curve).

Figure 12. The ratio to Rutherford cross section for ^{12}C+^{12}C scattering at $E_{\rm cm} = 7.998$

MeV. The solid curve shows the fit found with the model potential.

Figure 13. Inversion potentials from S matrix elements for $^{12}C+^{12}C$ at $E_{cm} = 7.998$ MeV. The results found using only physical phase shifts ($\Delta\ell = 2$ top panel) and using a complete set ($\Delta\ell = 1$ bottom panel) are compared to the fitted input potential (from which the S^ℓ were defined).

Figure 14. S matrix elements to the inversion potential (circles connected by dashed lines) compared to the input S matrix elements (crosses connected by full lines) in the Argand-diagram. The results were found using the potentials shown in Fig. 13.

FIGURES

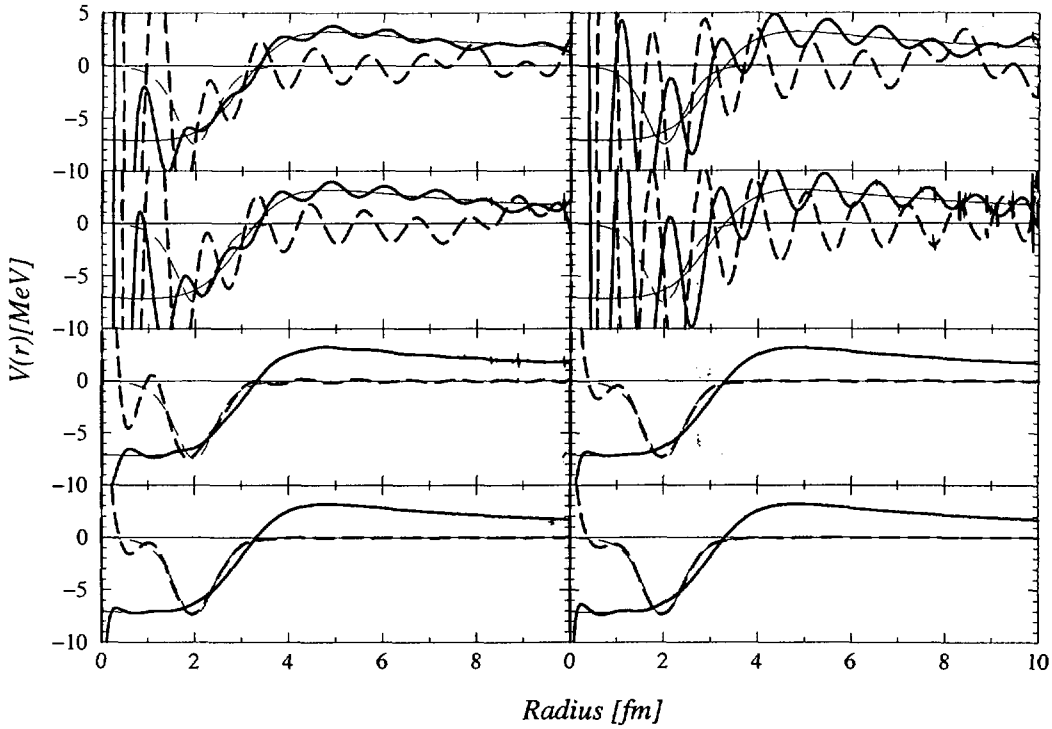

FIG. 1.

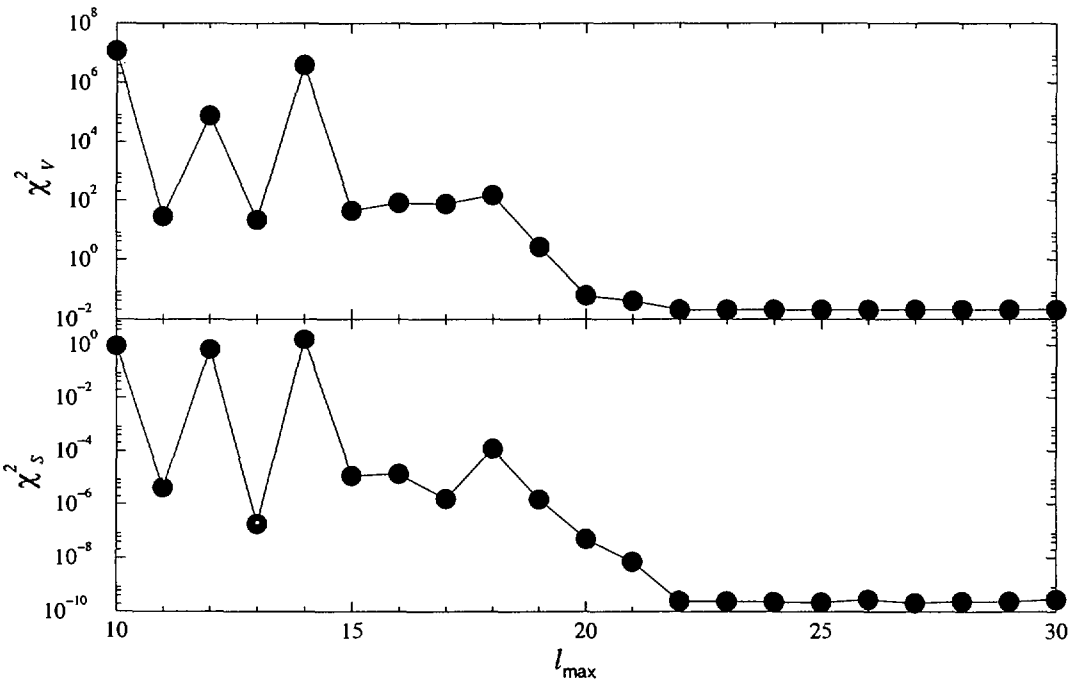

FIG. 2.

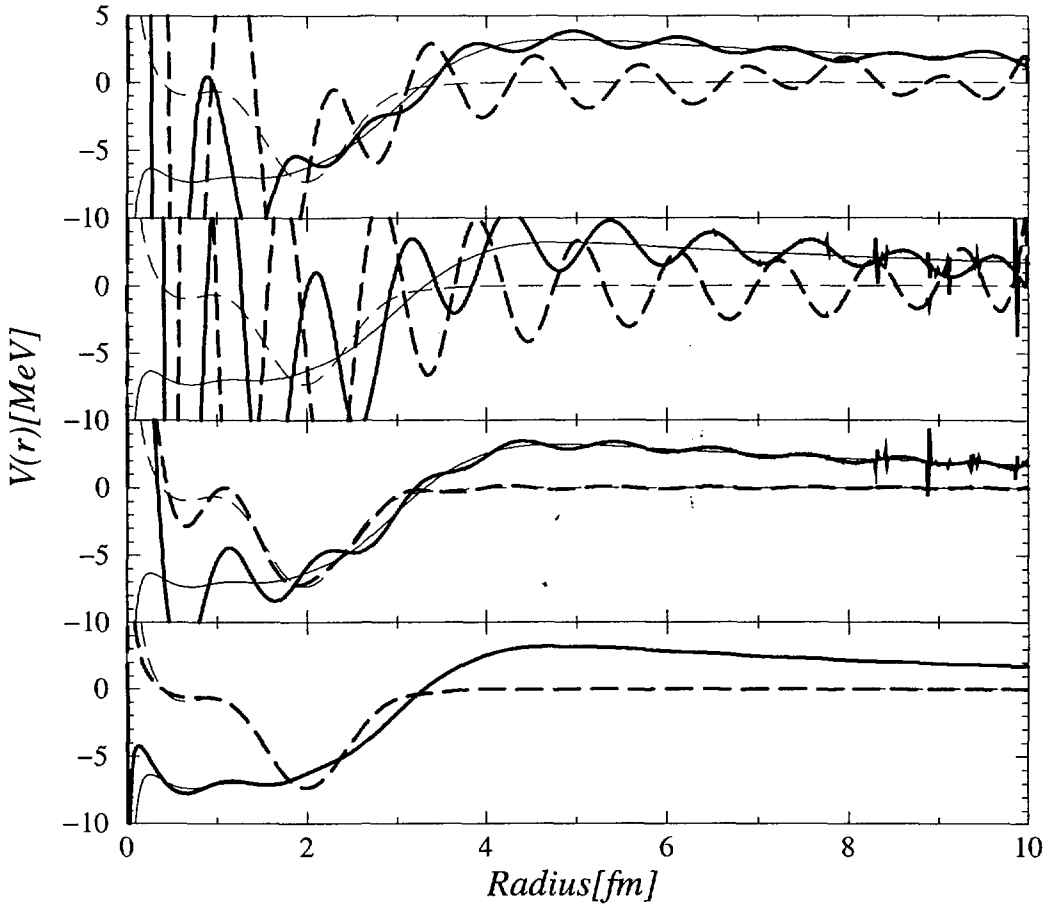

FIG. 3.

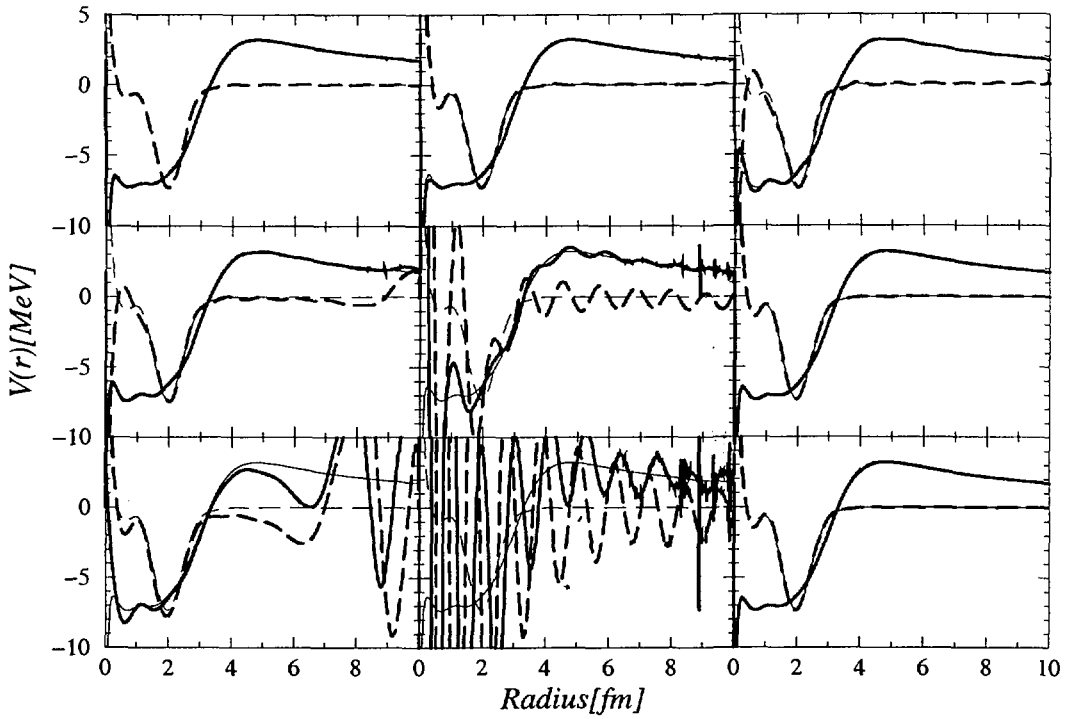

FIG. 4.

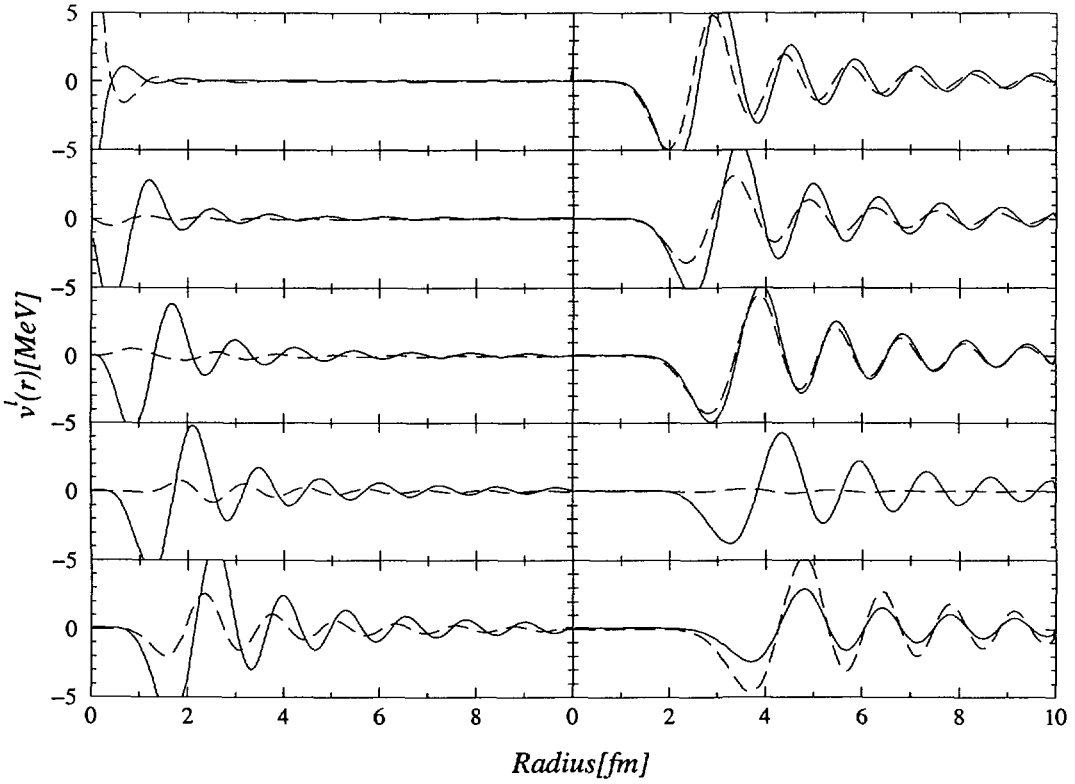

FIG. 5.

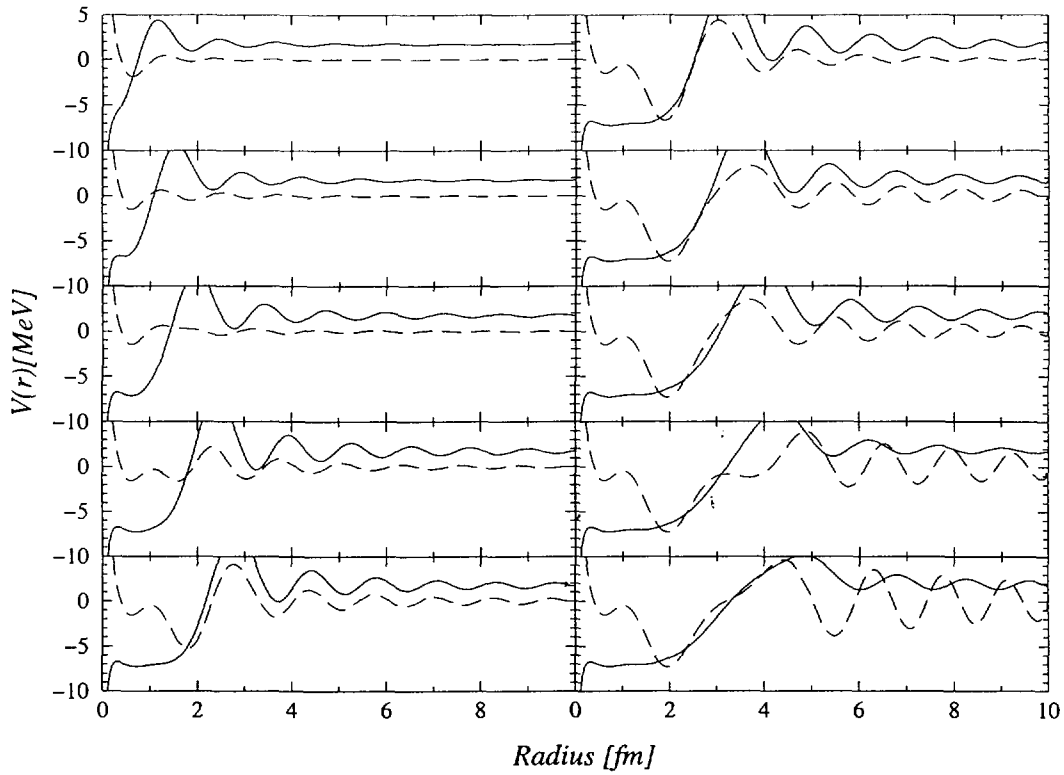

FIG. 6.

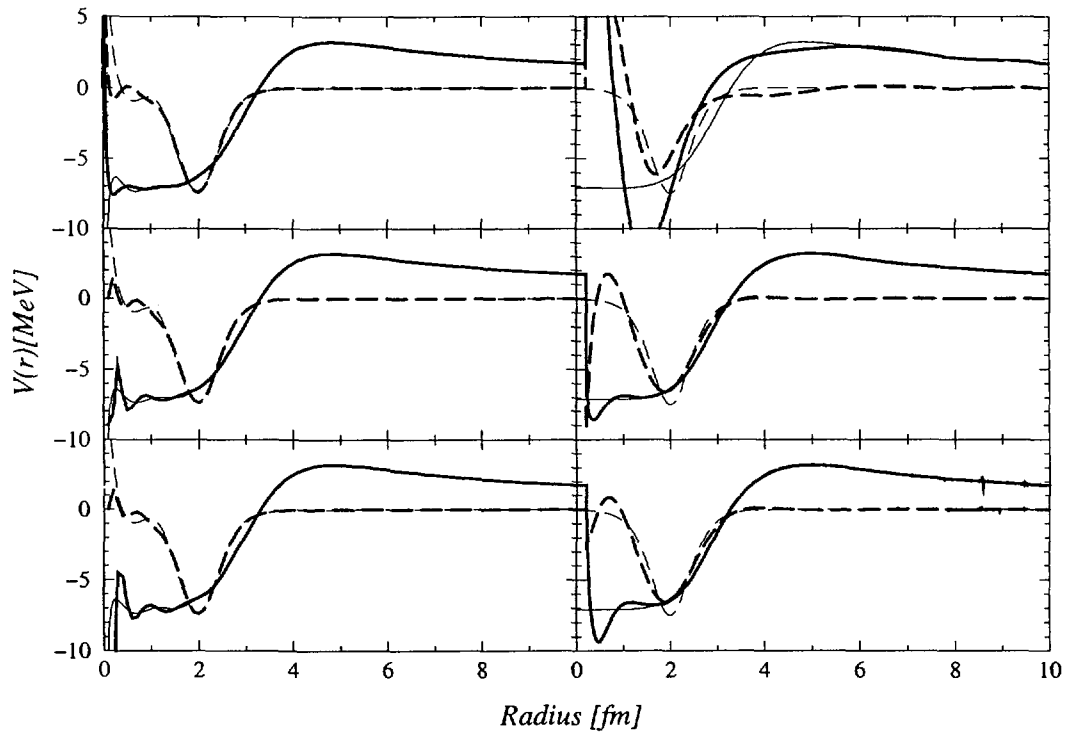

FIG. 7.

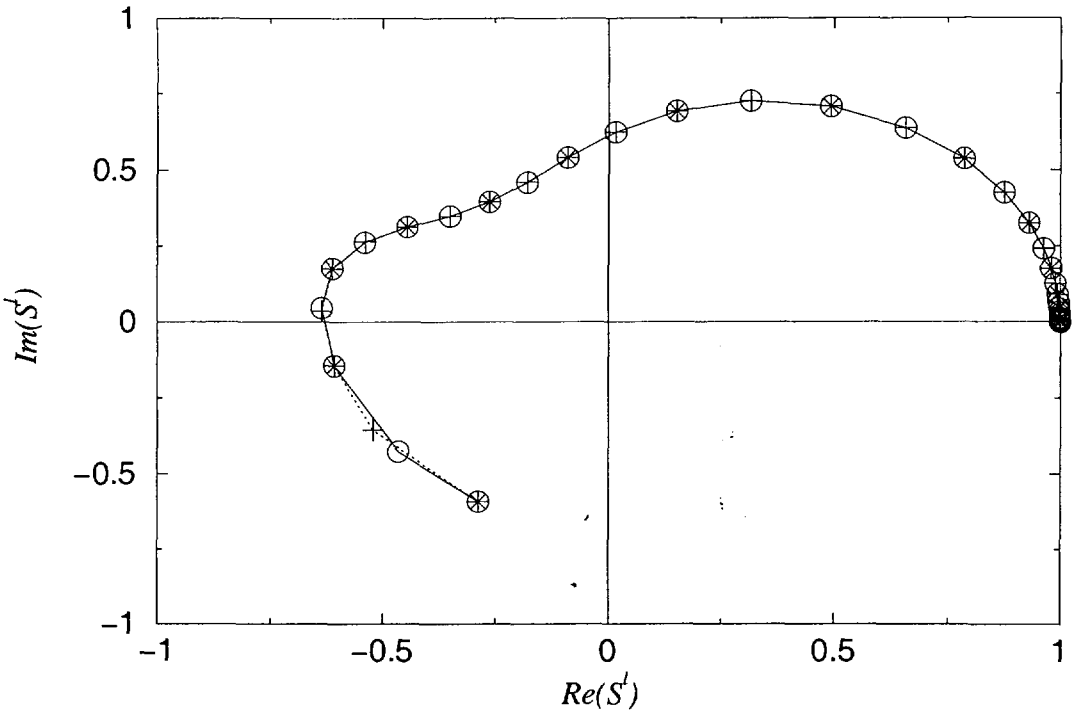
1
0.5
0
−0.5
−1
−1
−0.5
0
0.5
1
Im(S^l)
Re(S^l)

FIG. 8.

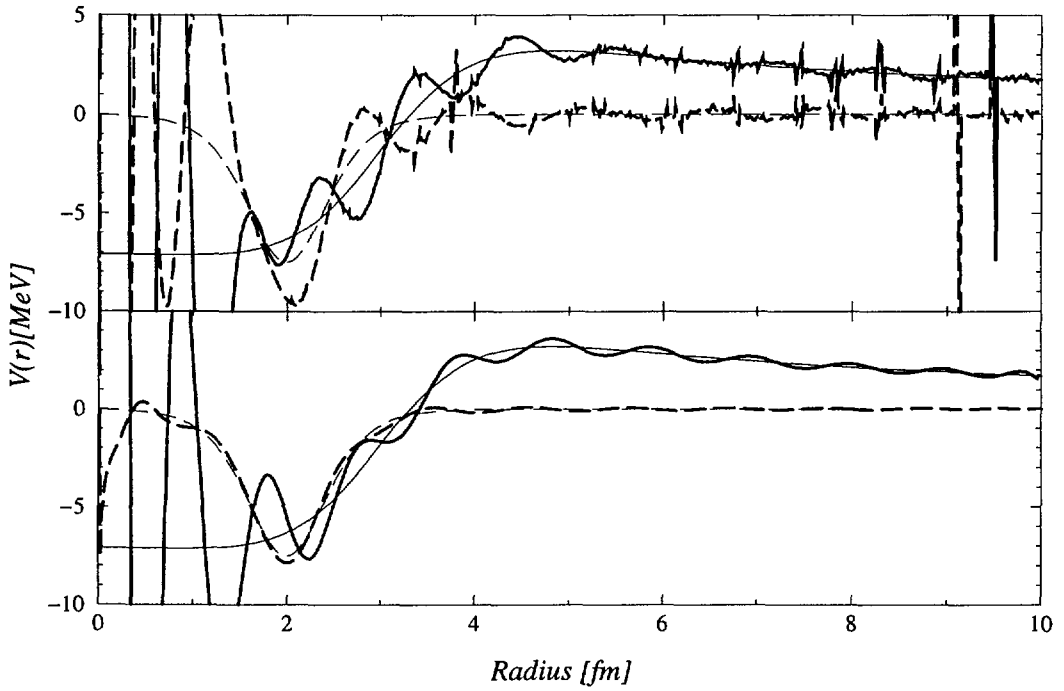
5
0
−5
−10
0
−5
−10
0
2
4
6
8
10
V(r)[MeV]
Radius [fm]

FIG. 9.

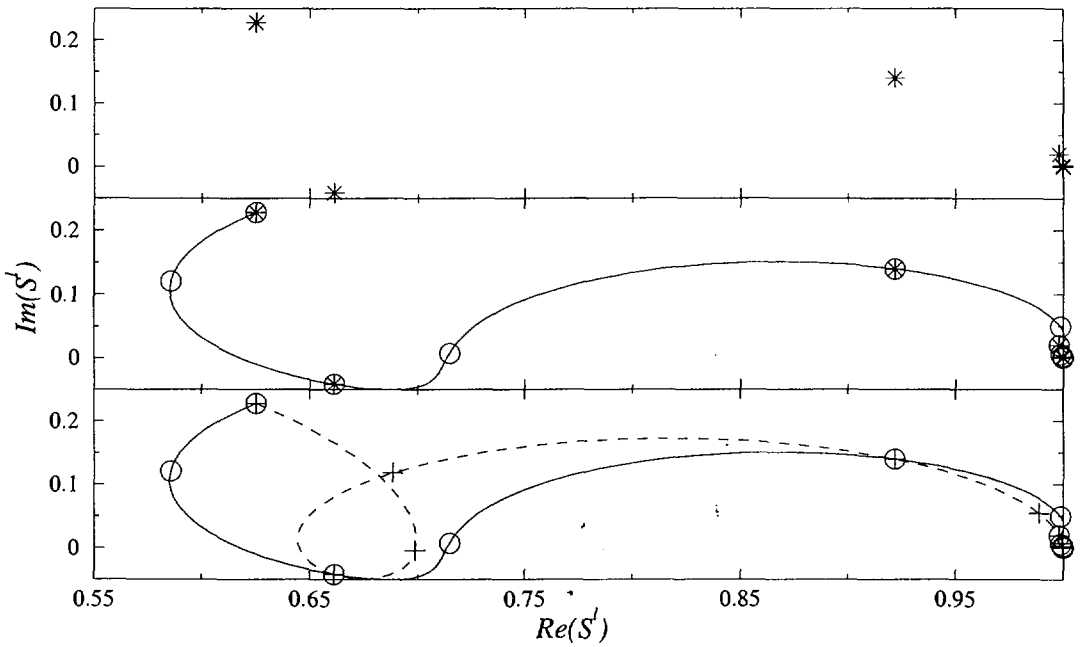
0.2
0.1
0
0.2
0.1
0
0.2
0.1
0
Im(S^l)
0.55
0.65
0.75
0.85
0.95
Re(S^l)

FIG. 10.

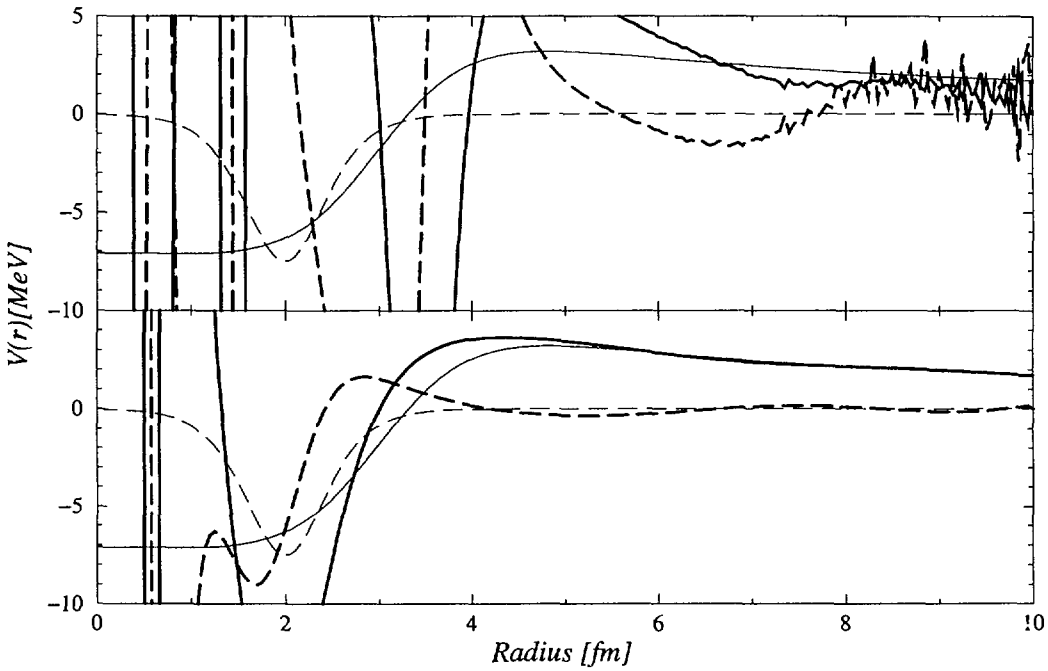
5
0
-5
-10
0
-5
-10
V(r)[MeV]
0
2
4
6
8
10
Radius [fm]

FIG. 11.

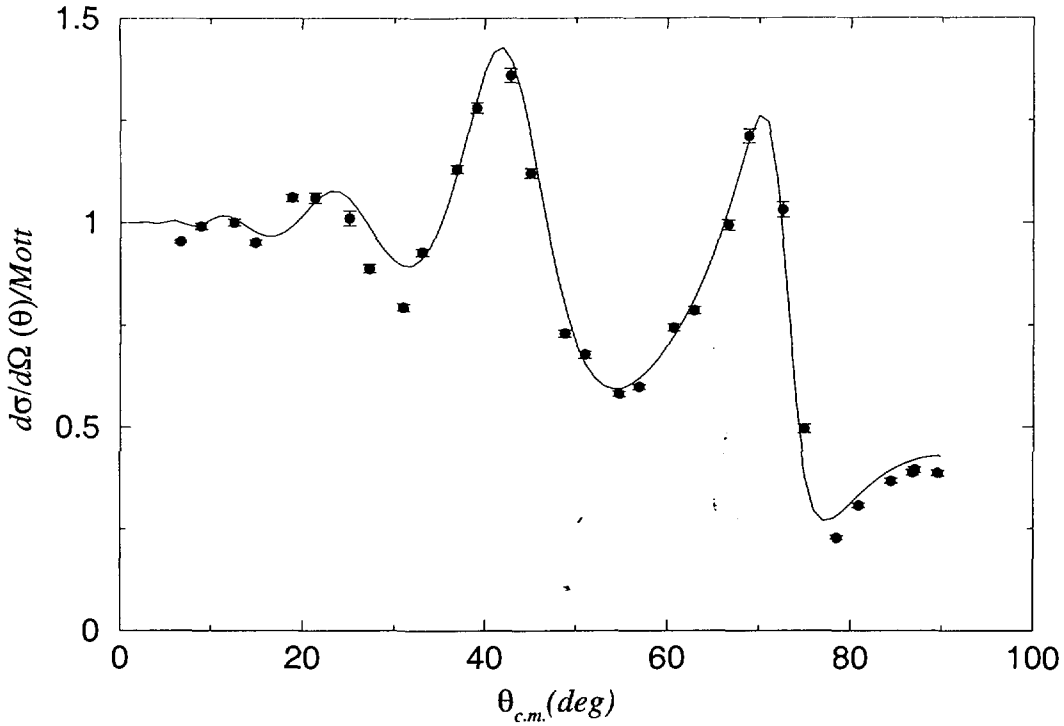
1.5
1
0.5
0
0
20
40
60
80
100
dσ/dΩ (θ)/Mott
θc.m.(deg)

FIG. 12.

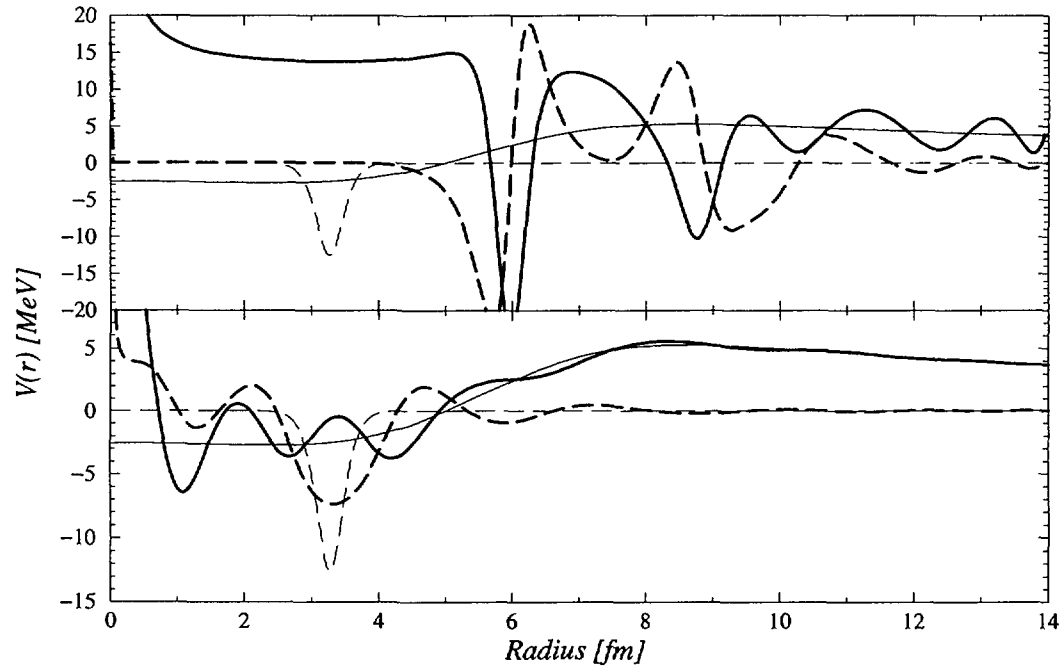
20
15
10
5
0
−5
−10
−15
−20
5
0
−5
−10
−15
0
2
4
6
8
10
12
14
V(r) [MeV]
Radius [fm]

FIG. 13.

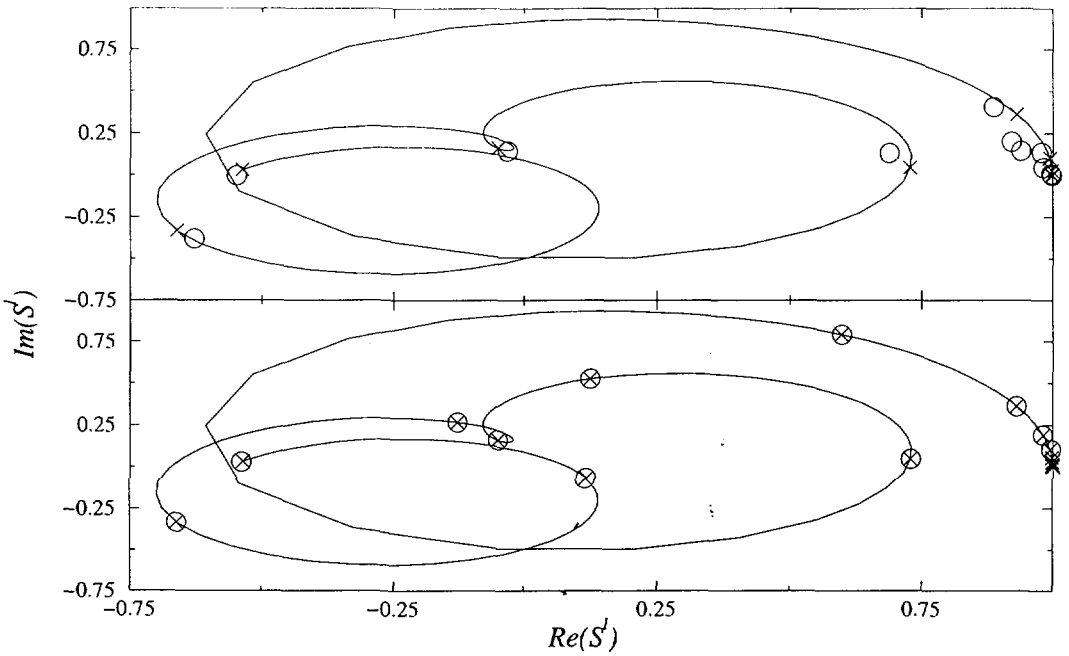

FIG. 14.